CrossMark

# The Bright Single Pulse Emission from PSR B1133+16

Jun Tan[1], Zhi-Gang Wen[2] , Zhen Wang[2,3], Xue-Feng Duan[2], Hong-Guang Wang[2,4], Na Wang[2], Vishal Gajjar[5] ,
Jian-Ping Yuan[2], Rai Yuen[2], Wen-Ming Yan[2] , Jian-Ling Chen[6], Wei Han[2], Hui Wang[6], Cheng-Bing Lyu[4], and Ai-Jun Dong[7]

[1] Maths and Information Technology School, Yuncheng University, Yuncheng 044000, China
[2] Xinjiang Astronomical Observatory, Chinese Academy of Sciences, Urumqi 830011, China; wenzhigang@xao.ac.cn
[3] Xinjiang Key Laboratory of Radio Astrophysics, Urumqi 830011, China
[4] School of Physics and Materials Science, Guangzhou University, Guangzhou 510006, China
[5] Space Science Laboratory, University of California, Berkeley 94710, USA
[6] Department of Physics and Electronic Engineering, Yuncheng University, Yuncheng 044000, China
[7] School of Physics and Electronic Science, Guizhou Normal University, Guiyang 550025, China

## Abstract

We have conducted a comprehensive investigation into the bright single pulse emission from PSR B1133+16 using the Giant Metrewave Radio Telescope. High time resolution data (61 $\mu$s) were obtained at a center frequency of 322 MHz with a bandwidth of 32 MHz over a continuous observation period of 7.45 hr. A total of 1082 bright pulses were sporadically detected with peak flux densities ranging from 10 to 23 times stronger than the average pulse profile. However, no giant pulse-like emission with a relative pulse energy larger than 10 and extremely short duration was detected, indicating that these bright pulses cannot be categorized as giant pulse emission. The majority of these bright pulses are concentrated in pulse phases at both the leading and trailing windows of the average pulse profile, with an occurrence ratio of approximately 2.74. The pulse energy distribution for all individual pulses can be described by a combination of two Gaussian components and a cutoff power-law with an index of $\alpha = -3.2$. An updated nulling fraction of $15.35\% \pm 0.45\%$ was determined from the energy distribution. The emission of individual pulses follows a log-normal distribution in peak flux density ratio. It is imperative that regular phase drifting in bright pulse sequence is identified in both the leading and trailing components for the first time. Possible physical mechanisms are discussed in detail to provide insights into these observations.

*Key words:* (stars:) pulsars: general – (stars:) pulsars: individual (PSR B1133+16) – methods: observational –
methods: data analysis

## 1. Introduction

Giant pulses, as one of the most remarkable radio emissions, are defined as pulses with intensity of thousands of times brighter than the average pulse profile, and with a duration much shorter than the so-called subpulses (Hankins et al. 2003; Karuppusamy et al. 2012). The discovery of the Crab pulsar was made possible by its emission of giant pulses (Staelin & Reifenstein 1968). Individual giant pulses originate from coherent emission mechanism with brightness temperature reaching as high as $10^{37}$ K (Cordes et al. 2004). These pulses are characterized by their very short duration, typically lasting only a few microseconds to milliseconds. The distribution of giant pulse energy could be described by a power-law distribution (Bhat et al. 2008), while the regular pulses follow log-normal statistics (Wen et al. 2022), which suggests that the giant pulses are distinct from regular pulses (Johnston & Romani 2002). Currently, there are several pulsars reported to exhibit giant pulse emission, including millisecond pulsars (Romani & Johnston 2001; Joshi et al. 2004; Knight et al. 2005) and young pulsars (Johnston & Romani 2003;

Hankins & Eilek 2007). Giant pulses with energy more than 5000 times that of the average pulse energy were detected from an extragalactic pulsar in the Large Magellanic Cloud, PSR B0540−69, at 1.38 GHz (Johnston & Romani 2003). Johnston & Romani (2004) argued that the power-law statistics give the best definition of giant pulses and speculated that giant pulses are associated with non-thermal high energy emission by briefly reviewing observational manifestations of pulsars with giant pulse emission. The magnetic field at the velocity light cylinder ($B_{\rm LC}$) has been proposed to be an indicator of giant pulse emissivity (Cognard et al. 1996; Knight et al. 2005), which is given as

$$B_{\rm LC} = 9.2\left(\frac{P}{\rm s}\right)^{-5/2}\left(\frac{\dot{P}}{10^{-15}\,{\rm s\ s^{-1}}}\right)^{1/2}{\rm G}, \qquad (1)$$

where $P$ and $\dot{P}$ are the pulsar rotational period and first period derivative, respectively. The pulsars confirmed with giant pulse emission possess higher values of $B_{\rm LC}$ than other pulsars, and $B_{\rm LC}$ turns out to be on the order to $10^{5-6}$ G. Istomin (2004) suggested that the plasma near the light cylinder is unstable

with respect to the reconnection of magnetic field lines. Thus, the origin of giant pulse emission can be traced back to the outer magnetosphere, and the giant pulses are generated by electric discharge and particle acceleration near the light cylinder.

In addition to giant pulses, some normal pulsars with rotation period ranging from 0.1 to a few seconds are detected to emit bright pulses which are stronger than average for a given pulsar but do not reach the extreme intensities of giant pulses (e.g., PSRs B0031−07, J1752+2359, B1112+50, B0656+14 and B0950+08) (Kuzmin & Ershov 2004; Ershov & Kuzmin 2005; Weltevrede et al. 2006; Singal & Vats 2012). Such bright single pulses are typically distinguished by peak fluxes stronger than ten times the peak of average flux density, which is not equivalent in practice to the canonical giant pulse definition with ten times the pulse energy implemented by Burke-Spolaor et al. (2012). The emission from these pulsars displays the distinct characteristics seen in giant pulses in terms of pulse width. The duration of bright pulses can vary widely depending on the pulsar itself and specific observational parameters. They may last from milliseconds to several seconds. Furthermore, the pulsars detected with bright pulses possess low values of $B_{LC}$, typically lower than 1000 G. The bright pulses are proposed to be part of the regular emission from pulsars, which is caused by the acceleration of charged particles along magnetic field lines and the subsequent emission of electromagnetic radiation (Wen et al. 2021). The exact physical mechanisms behind giant pulses and bright pulses are not fully understood, but they are believed to involve highly energetic processes in the pulsar's magnetosphere, and are thought to be related to the pulsar's magnetic field and its interaction with charged particles.

PSR B1133+16, one of the brightest isolated radio pulsars in the Northern hemisphere (with a flux density of 257 mJy at 400 MHz according to the ATNF Pulsar Catalogue[8]), has served as a fascinating target for the exploration of various emission phenomenon. Analysis of the individual pulse behavior has revealed a variety of characteristics across different observing frequencies spanning from 18 MHz to 8.35 GHz (Backer 1973; Herfindal & Rankin 2007; Honnappa et al. 2012). A low-frequency feature linked to amplitude modulation associated with the pulse-to-pulse intensity fluctuations is modulated at the frequency of $f_4 \simeq 0.033P^{-1}$, which can be regarded as the circulation time of $P_4 \simeq 30P_1$ under the subbeam rotating carousel model (Honnappa et al. 2012). The phenomenon of subpulse drifting is apparent in PSR B1133+16 as well. Additionally, a high-frequency feature originating from phase modulation was identified by Weltevrede et al. (2007), corresponding to a period of $P_3 = (3 \pm 2)P_1$. The complete cessation of emission, typically lasting only a single period and never exceeding four periods, was observed to occur approximately 15% of the time (Herfindal & Rankin 2007).

PSR B1133+16 is recognized as a bright pulsed source at multiple frequencies (Kramer et al. 2003; Herfindal & Rankin 2007; Karuppusamy et al. 2011) as well. Anomalously strong (giant) pulses from this pulsar were detected at a frequency of 111 MHz using the Large Phased Array radio telescope (Kazantsev & Potapov 2015). The most intensive individual pulse had a peak flux density 86 times that of the dynamic averaged profile and a duration of 0.2 times the average profile duration. Ulyanov et al. (2006) reported the presence of strong subpulses with peak intensity 20 times greater than the peak intensity of the mean profile detected at the decameter wavelength range (18–30 MHz).

Despite extensive detection of bright pulses, the underlying mechanism behind their occurrence in PSR B1133+16 remains elusive. Moreover, a clear differentiation between classical giant pulses and bright pulses has not been attempted. Therefore, it is crucial to investigate the fundamental nature of the pulsar's bright pulses in order to gain deeper insights into the physical processes within its magnetosphere.

This paper presents the results of a comprehensive study on the prominent bright single pulses from PSR B1133+16. We conducted high-quality single-pulse observations using Giant Metrewave Radio Telescope (GMRT) at a frequency of 322 MHz. The details of observations and data processing procedures are presented in Section 2. The obtained results are presented in Section 3. The implications and interpretations of these findings are discussed in Section 4. Finally, in Section 5, we provide a summary of our study and draw conclusions based on the results obtained.

## 2. Observations and Data Reduction

The observations were carried out with the GMRT on 2013 August 11. The GMRT comprises 30 dish antennas, each with a diameter of 45 m (Swarup et al. 1991). The single-beam phased array mode, incorporating all central square antennas, was employed to reduce the fluctuations in phase differences induced by the ionosphere. The observations were conducted by operating the legacy GMRT 32 MHz bandwidth system at the central frequency of 322 MHz (Roy et al. 2010). The digitized signals from each antenna were summed coherently in phase with the GMRT Array Combiner. The data streams were processed with the GMRT Software Backend (GSB). Then, the combined signals were partitioned into 512 spectral channels via the GMRT correlator, with each channel having a bandwidth of 62.5 KHz. The data were acquired into a 16-bit output buffer every 61 $\mu$s. Details on the observational configuration are described in Bhattacharyya et al. (2013, 2021).

The data from GMRT observations were converted into the standard filterbank format which is required for the Pulsar Signal Processing Programs (SIGPROC[9]) analysis package.

---

[8] http://www.atnf.csiro.au/research/pulsar/psrcat/
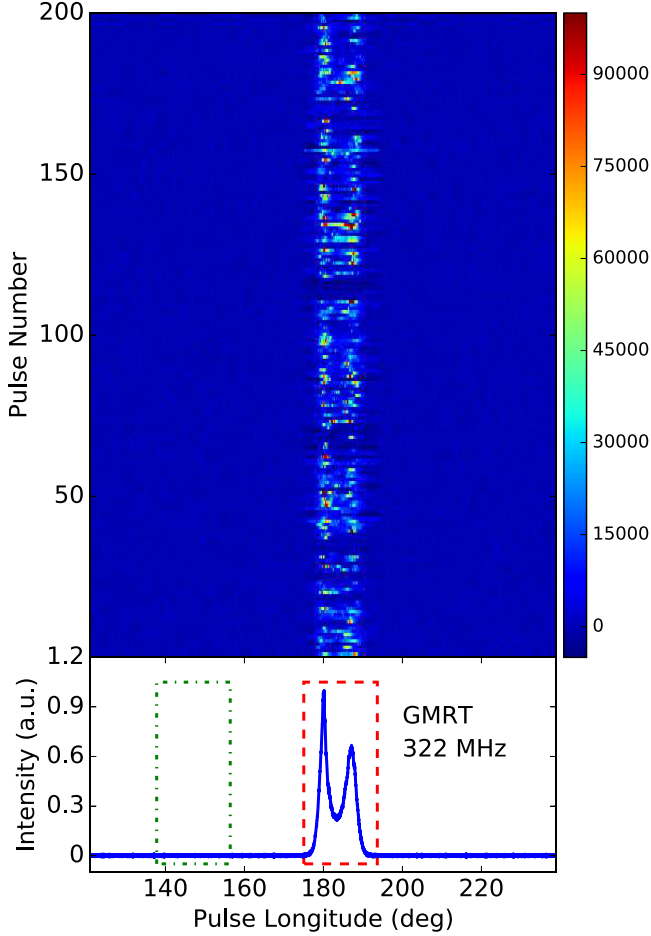
[9] http://sigproc.sourceforge.net/

**Figure 1.** A typical sequence of 200 successive individual pulses of PSR B1133+16 obtained from the GMRT observations at 322 MHz. The abscissa is the rotational longitude of the pulsar. The upper panel displays a stack of individual pulses using a color map that ranges in intensity from blue to red. The presence of null pulses is clearly evident between the burst pulses. The integrated pulse profile is presented in the bottom panel. The dashed square shows the on-pulse window, while the dash–dotted square displays the off-pulse window.

The raw lterbank data from each channel were incoherently dedispersed at the dispersion measure (DM) of the pulsar (DM = 4.84 pc cm$^{-3}$) to correct for the frequency-dependent spread caused by the dispersive effects of the plasma (Lorimer & Kramer 2012). Using the pulsar ephemerides from the ATNF Pulsar Catalogue (Manchester et al. 2005), the dispersion-corrected data are folded into single-pulse time series at the topocentric spin period. A typical single pulse sequence after de-dispersion and folding is shown in the top panel of Figure 1. One can see that the strong pulse peaks and nulls are distinguished by magenta and blue respectively.

Subsequently, the data underwent a search for bright pulses, with single pulses having a signal-to-noise ratio exceeding 5 being selected as candidates. From the GMRT data observed at
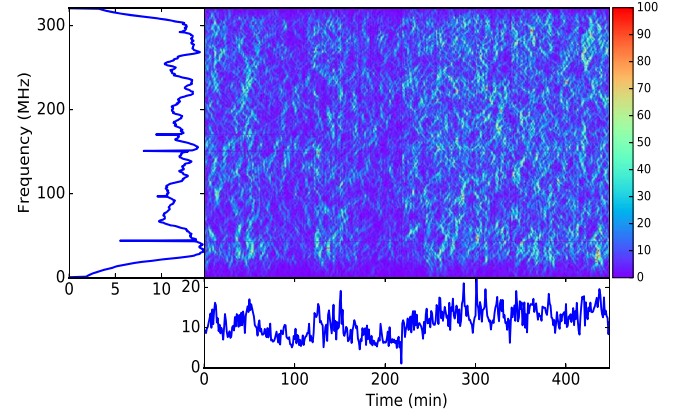


**Figure 2.** The dynamic spectrum of scintillation for PSR B1133+16, observed with GMRT at 322 MHz. Here the measured on-pulse energy of the pulsar signal is plotted as a function of both time and frequency. The left-hand and bottom panels present the power integrated over frequency and time, respectively.

322 MHz, a total of 1082 bright pulses were identified, each possessing a peak flux density greater than 10 times that of the dynamic mean profile. Our observation spanned a continuous period of 7.45 hr, and we achieved a detection efficiency of one bright pulse in every 20 pulse periods. These results highlight the robustness of our identification process and provide valuable insights into the occurrence and characteristics of bright pulses in the PSR B1133+16 data set.

## 3. Results

### 3.1. Pulse Energy Distribution

The diffractive interstellar scintillation for PSR B1133+16 is quite severe, which corrugates the intensity in time and frequency domain, because it is close to the Earth with low DM of 4.84 pc cm$^{-3}$. The dynamic spectrum at 322 MHz, as depicted in Figure 2, shows scattered bright patches known as scintles distributed across the plot. In accordance with the thin screen approximation within the interstellar medium, the decorrelation bandwidth (representing the characteristic frequency scale of the scintles) scales proportionally to $\nu^{4.4}$, while the characteristic timescale scales proportionally to $\nu^{1.2}$, where $\nu$ is the observing frequency (Bhat et al. 2004). Under the assumption of Kolmogorov scaling, the scintles are expected to exhibit a characteristic timescale of 503.3 s and a scintillation bandwidth of 15.7 MHz, which corresponds to half the observing bandwidth (33 MHz) at 322 MHz (Cordes & Lazio 2002). Consequently, the intensity fluctuations induced by scintillation is invisible in frequency.

In order to compare the bright pulses of PSR B1133+16 with the normal pulses, the pulse energy distribution is interpreted carefully to refrain from over- and underestimation caused by interstellar scintillation. To address the intensity
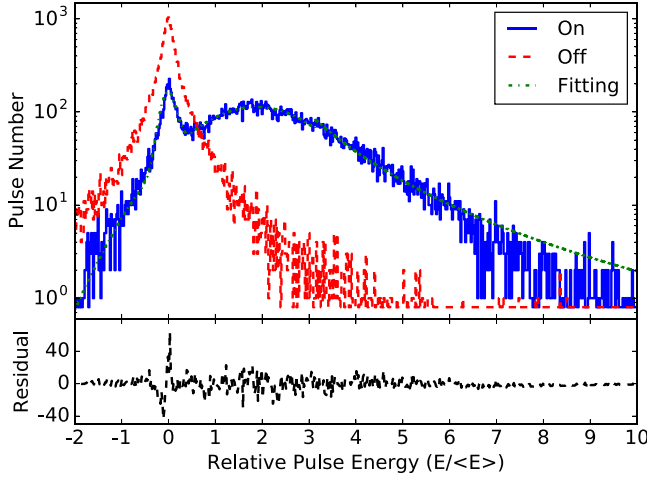
**Figure 3.** Histograms of the scintillation-corrected and normalized on-pulse (solid line) and the off-pulse (dashed line) energies for PSR B1133+16 observed from the GMRT at 322 MHz. It shows clear nulling with a distinctly separate null and burst pulses among the on-pulse energy distribution. The estimated NF is around $15.35\% \pm 0.45\%$. The dash–dotted line represents the on-pulse energy fitting based on the combination of two Gaussian components and a cutoff power-law with index of $-3.2$. The residuals from the best fitting are shown in the bottom panel.

fluctuations over time, the pulse energies are normalized by comparing them to a running average of 500 pulse energies, spanning a duration longer than the scintillation timescale. This approach is favored over simply averaging the pulse energy from the entire observation. Additionally, the on-pulse and off-pulse windows, each possessing an equal width of pulse longitude as indicated in Figure 1, are selected from the integrated pulse profile to generate the on-pulse energy and off-pulse energy sequences, respectively.

Figure 3 illustrates the histograms of the scintillation-corrected and normalized on-pulse and off-pulse energies. The energy distribution during the on-pulse extends across an exceedingly broad range of energy levels. The histogram formed from off-pulse energies (dashed line) predominantly centers around zero. In contrast, the histogram of on-pulse energies (solid line) displays a narrow Gaussian component within the zero energy bin, attributable to the presence of null pulses, along with a long tailed component due to burst pulses. As we can see, the best-fit solution gives us a distribution of the on-pulse energy for all individual pulses as a combination of two Gaussian components and a cutoff power-law characterized by an index of $-3.2$. However, it is noteworthy that no pulses with relative pulse energies exceeding 10 are detected, which aligns with the standard operational definition of giant pulses (Hankins et al. 2003).

A similar shape of the distribution for the pulse energy histogram was previously obtained at 408 MHz (Ritchings 1976). In order to determine the nulling fraction (NF), a method

akin to that employed by Ritchings (1976) and Vivekanand (1995) has been adopted for this pulsar. The estimated NF is $15.35\% \pm 0.45\%$, which is consistent with the result given by Herfindal & Rankin (2007) at 327 MHz.

## 3.2. Bright Pulse Emission

We have identified bright single pulses at phases corresponding to the leading, saddle, and trailing emission components of the pulsar, as illustrated individually in Figure 4. Notably, the peak flux density of the strongest pulse is approximately 23 times brighter than that of the average pulse profile (upper left subplot). The leading and trailing components both with peak flux density exceeding 10 times that of the average pulse profile are shown in the lower right plot simultaneously. The plots reveal the presence of micropulses characterized by ultrashort intensity variations within individual pulses. In Figure 5, we present the average profile obtained by integrating all individual pulses at 322 MHz, along with a histogram depicting the number of bright pulses in the upper panel. The distribution of the 1082 bright pulses is depicted in the lower panel, indicating a notable preference for these bright pulses to align within the narrow windows of the leading and trailing components. Additionally, several bright pulses are observed to be located within the saddle component. It is worth highlighting that the width of the strongest individual pulse accounts for approximately 10% of the width of the average profile.

Recently, there have been discoveries of several pulsars displaying quasi-periodic transitions between null and burst states. Herfindal & Rankin (2007) also noted a low-frequency intensity fluctuation occurring at intervals of 32 pulses. While periodic analyses have been conducted on null states, no similar investigations have been undertaken regarding bright pulse emissions. Following the method to describe the quasi-periodic nulls, a sequence representing two emission states is formed by designating bright pulses as ones and all remaining pulses (normal pulses and nulls) as zeros. Subsequently, a Fourier Transform is carried out on the state sequence to assess the presence of any underlying periodic patterns. However, the Fourier spectrum analysis did not reveal any significant periodic signals.

In accordance with the established practice of previous studies on pulsars exhibiting bright pulse emission, the ratio of peak flux density distribution is computed. The histogram illustrating this distribution is shown in Figure 6. It is noted that the peak flux density ratio could be best represented by a log-normal distribution by using a least-squares fitting approach. The dashed line is the best log-normal fit with the logarithmic mean value of 0.81 and the standard deviation of 1.15.

The scatter plot of the peak flux density ratio and the half-power width ($W_{50}$) is shown in Figure 7. It is clear that the $W_{50}$ of bright pulses has a bimodal distribution ranging from $0°\!.06$
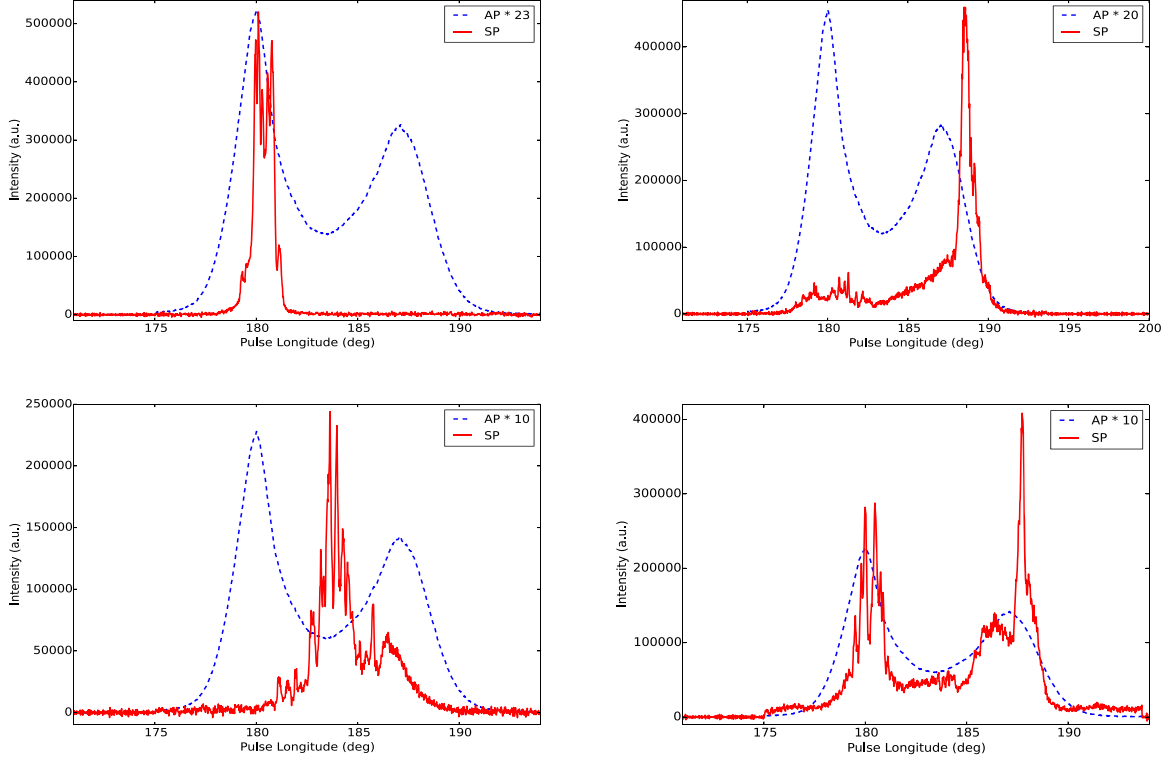
**Figure 4.** A comparison of the bright single pulses and the averaged pulse profile of PSR B1133+16 obtained at 322 MHz with GMRT is presented with solid and dashed lines, respectively. The averaged pulse profiles are multiplied by 23, 20, 10 and 10, as expressed in the figure legends respectively. The bright pulses are presented in the leading (upper left, the strongest pulse), saddle (lower left) and trailing (upper right) components of the mean pulse profile individually. The leading and trailing components both with peak flux density above 10 times the average pulse profile are shown in the lower right plot.
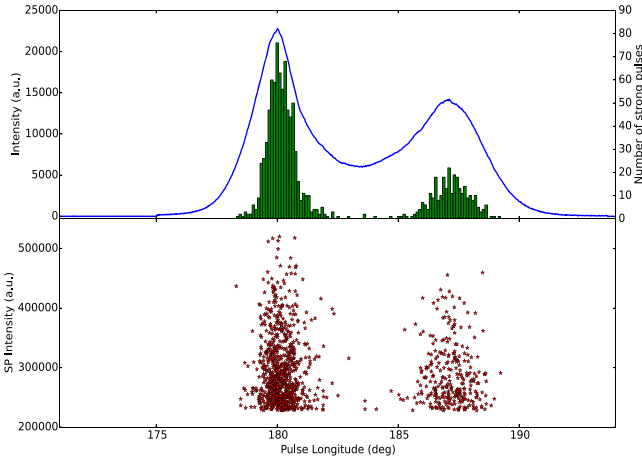


**Figure 5.** Average pulse profile obtained from GMRT data, as well as the histogram of the number of bright pulses, is presented in the upper panel. The distribution of 1082 bright pulses is shown in the lower panel. The units of intensity in the two panels are arbitrary.
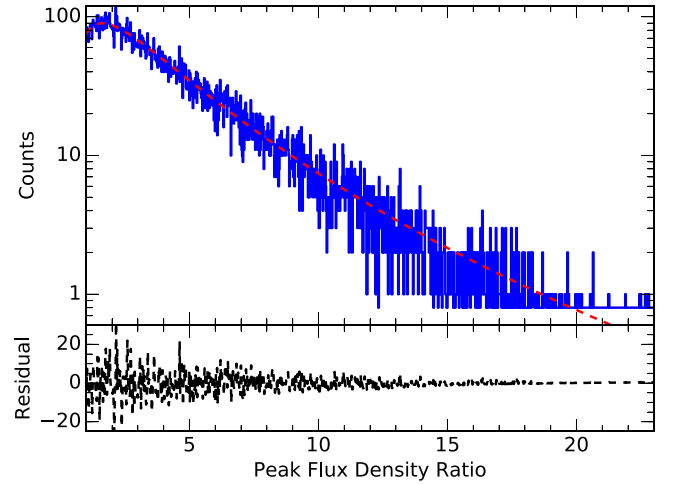


**Figure 6.** Distribution of the peak flux density of single pulses relative to that of the mean pulse profile. The best-fitting log-normal function is shown as a dashed line. The residuals are shown in the lower panel.

to $9°.74$, corresponding to approximately 0.20–32.14 ms. For comparison, the $W_{50}$ for the integrated pulse profile is about $9°.12$. Furthermore, no strong correlation is found between peak flux density ratio and pulse width.

The normalized average pulse profiles of all individual pulses (solid line), the 1082 bright pulses (dashed line) and the profile produced by individual pulses with bright pulses removed (dash–dotted line) are shown in Figure 8. The shapes
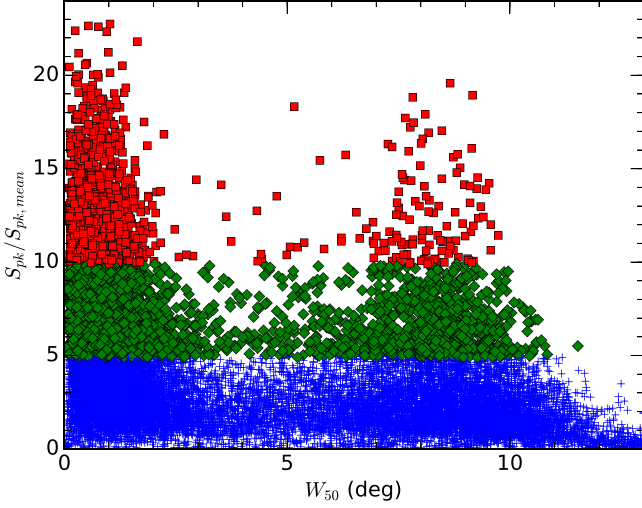
**Figure 7.** Peak flux density ratio versus half-power width for the individual pulses with signal-to-noise ratio larger than 5. Strong and normal pulses are labeled with squares and plus symbols respectively.



**Figure 8.** The normalized average pulse profile of all individual pulses (solid line) and that of 1082 strong pulses (dashed line) and profile produced by individual pulses without strong pulses (dash–dotted line).

of the pulse profiles are relatively simple, featuring well-resolved main emission components connected by a pronounced intermediate saddle emission, as documented by Ji-Guang et al. (2015). Importantly, all pulse profiles are aligned without shifts in pulse longitude. The strong pulse profile is slightly narrower, while the saddle and trailing components exhibit intensity reductions by approximately 66% and 34%, respectively, compared to those of a normal pulse profile. Subsequent two-sample Kolmogorov–Smirnov statistical tests are applied on the above profiles, indicating discernible differences in their distributions, as evidenced by all $p$-values falling below 1%.

### 3.3. Regular Phase Drifting in Bright Pulses

It is well known that many pulsars are recognized for displaying systematic drifts of subpulses across the emission window during normal pulse emission. To explore whether the bright pulses present similar phase modulation characteristics for PSR B1133+16, the bright pulses with longitude located in the leading and trailing components are selected to form two pulse sequences in chronological order, respectively. In the investigation, a sequence of 793 bright pulses with peak longitude in the range of 175°.0 to 183°.4 is depicted in the upper panel of the left plot in Figure 9. Additionally, the upper panel of the right plot presents a sequence of 289 bright pulses with peak longitude ranging from 183°.4 to 193°.6. The integrated pulse profiles for both sequences are illustrated in the lower panels (solid lines). For comparison purposes, the pulse profile averaged over all single pulses is presented with a dashed line.
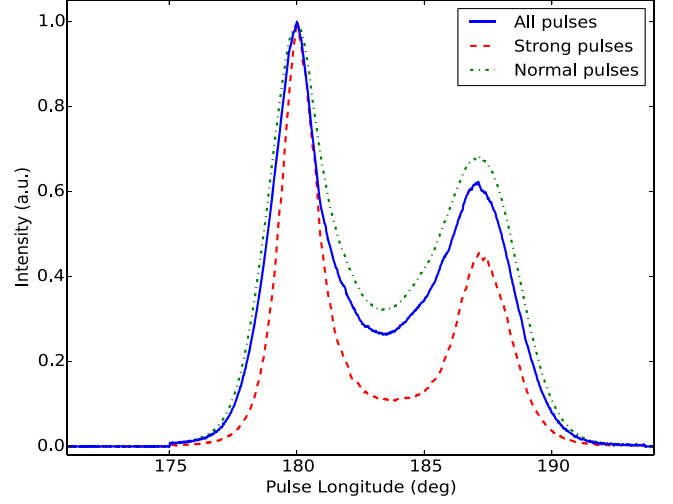
As we can see, the bright pulses in the leading component exhibit a remarkably organized and captivating modulation pattern: the phase of subpulse shifts progressively in successive bright pulses, which resembles the phenomenon of drifting subpulses observed in normal pulses. However, the apparent phase-stationary intensity modulations (stationary drift) are also observed at the beginning and end of the sequence. Such regular drifting is exclusively observed in the leading region, with no discernible drifting signature present in either the saddle region or the trailing region. Upon visual inspection of the regular phase variation behavior in bright pulses, seven distinct drift bands are clearly identified in the leading component. Table 1 summarizes the drift parameters shown in the left plot of Figure 9. Following the drift band number and the number of bright pulses in the first two columns, the horizontal time interval ($P_2$ in units of degree) and the vertical band spacing ($P_3$ in units of minute) are given in the last two columns.

In the sequence of trailing bright pulses, we also detect some degree of irregular phase drifting in both the leading and trailing components. The left-hand panels of the plot show the evolution of burst rate, which is derived from the number of bright pulses within every 400 successive single pulses. However, cross-correlation analyses conducted between burst rate, drifting phase, and burst intensity reveal no significant correlations.

## 4. Discussion

We show in this paper that the emission of PSR B1133+16 can be characterized by bright pulse emission. They are slightly strong compared to normal pulses and with peak flux density well above 10 times that of an average pulse profile. From Figure 7, the broad bimodal distribution is displayed in the
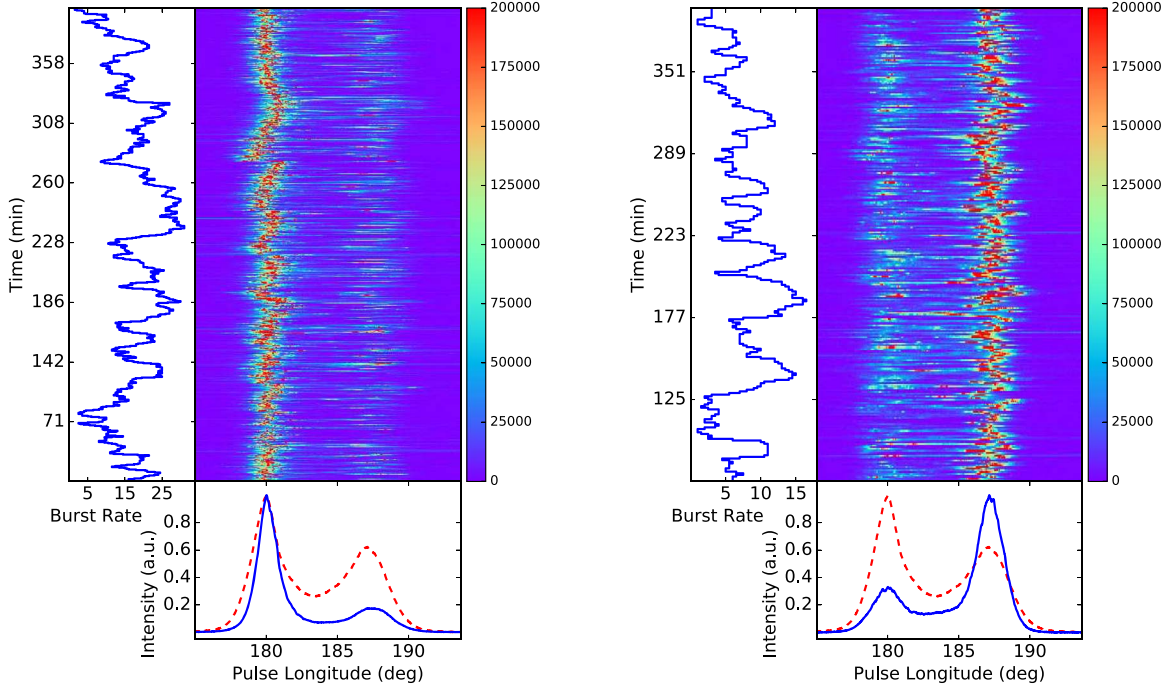
**Figure 9.** Sequences of separated bright pulses located in the leading (793 single pulses, left) and trailing (289 single pulse, right) components. The pulse profiles integrated by the above bright pulses are presented in the bottom panels with solid lines. For comparison, the pulse profile averaged over all single pulses is shown with a dashed line. The profiles are all normalized to one. The left panels show burst rate of bright pulses.

**Table 1**
Summary of Drift Parameters of Bright Pulses in the Leading Component

| Drift Band | Number of Bright Pulses | $P_2$ (deg) | $P_3$ (minute) |
|---|---|---|---|
| 1 | 46  | $0.47 \pm 0.17$ | 49.12 |
| 2 | 62  | $0.80 \pm 0.20$ | 30.19 |
| 3 | 88  | $0.72 \pm 0.20$ | 25.72 |
| 4 | 69  | $0.69 \pm 0.18$ | 20.41 |
| 5 | 65  | $1.08 \pm 0.15$ | 14.49 |
| 6 | 81  | $1.21 \pm 0.12$ | 26.27 |
| 7 | 110 | $1.74 \pm 0.21$ | 31.24 |

width of bright pulses, which is caused by the significant relative intensity fluctuation between leading and trailing components. In regard to the ultrashort duration of pulses dominated by microstructure, they are much broader than the extremely narrow giant pulses. The energy of regular pulses follows an exponential or log-normal distribution (Burke-Spolaor et al. 2012), whereas giant pulses are initially observed to conform to a power-law distribution (Ritchings 1976). For PSR B1133+16, a significant high-energy tail is shown, and could be described by a cut-off power-law with a slope of $\alpha = -3.2$. Therefore, the bright pulses from PSR B1133+16 cannot be sufficiently strong and narrow to be classified as giant pulses. However, it is noted that the bright pulses are located in the same pulse phase with normal pulses, which

confirms that both are emitted from the same inner gap of the magnetic polar region as the average pulse (Kuzmin & Ershov 2006). PSR B1133+16 shows the presence of double bright pulses in both the leading and trailing phases at 322 MHz, indicating that there are two emission regions of bright pulses. The pulsar magnetosphere is the region around the neutron star dominated by its magnetic field. The physical process or mechanism causing these bright pulses affects the entire magnetosphere of the pulsar, not just the localized regions. Although the bright pulses in the leading and trailing phases originated from physically distinct areas within the pulsar's magnetosphere, the underlying physical mechanism is widespread across the entire pulsar's magnetosphere rather than confined to a single region (Kuzmin & Ershov 2004; Karuppusamy et al. 2011).

There are also interesting parallels between bright pulse and giant pulse emission. The pulse longitudes exhibit notable constraints, either toward one edge or centrally located (Kuzmin & Ershov 2004; Tao et al. 2012). PSR B1133+16 and several other slowly-rotating pulsars with reported giant pulse emissions do not align with the purported empirical correlation between the occurrence of giant pulses and high light-cylinder magnetic field strength, since its value of $B_{\rm LC} \simeq 11.6$ G is well below those of most pulsars exhibiting classical giant pulses (around $10^5$ G) (Cognard et al. 1996). As a rule, pulsars exhibiting high values of the light-cylinder

magnetic field $B_{LC}$ are linked to high energy emission originating from the outer gaps. In the outer-gap model of high energy emission, Cheng et al. (1986) proposed that the X-ray and $\gamma$-ray pulses originate from the outer magnetosphere acceleration gap along the boundary of the open zone. For instance, a phase correlation of giant pulses with the high energy non-thermal $\gamma$-ray emission is displayed in the Crab pulsar (Lundgren et al. 1995). Enoto et al. (2021) found that the giant pulses from the Crab pulsar are associated with enhanced X-ray emission, implying that the high energy emission possibly originates close to the radius of the light cylinder with a high magnetic field. PSR B1133+16 shows non-thermal X-ray emission originating from the polar cap region (Kargaltsev et al. 2006), which could be related to the bright pulses we detected in this work. A deep search in the simultaneous X-ray and radio observations is necessary to reveal any more correlations.

The sporadic bright and giant pulses are so bright that they are hardly induced by intrinsical intensity-modulation of normal pulses or by the interstellar scintillation. In terms of the intensive emission, bright and giant pulses may arise due to various factors, such as enhanced pair production within the magnetosphere, heightened coherence of synchrotron emission, alterations in the direction of beaming, or induced Compton scattering in the flow of pulsar plasma (Petrova 2004). Malov (2022) assessed the applicability of established models proposed to explain giant pulses through a comparison of the parameters of the pulsars. It is widely accepted that giant pulses are generated within a vacuum region near the surface of a neutron star (Kontorovich 2009). The presence of this gap and the existence of electric fields within it are considered to be commonly acknowledged. Machabeli et al. (2019) suggested that the giant pulses are also attributed to nonlinear processes in plasma during the formation of drift waves at the outer edge of the pulsar's magnetosphere. Malov (2022) proposed that it appears to be heightened considering the potential use of the giant pulse phenomenon in explaining fast radio bursts. The energies of nonrepeating fast radio bursts are observed to show a power-law distribution with an index ranging from 1.6 to 1.8 (Luo et al. 2018, 2020; Wang et al. 2021; Zhang et al. 2021). The pulse energy of bright pulses and giant pulses also shows a power-law distribution. Li et al. (2021) found that the burst energy of a repeating fast radio burst source follows a bimodal distribution, and can be well characterized by a combination of a log-normal function and a generalized Cauchy function. The lower-energy component exhibits a distribution pattern similar to what is observed in numerous radio pulsars. On the other hand, the higher-energy end displays a tendency toward a power law with a slope resembling the characteristics of giant pulses emitted by the Crab pulsar. The underlying magnetospheric physics of bright and giant pulses may help to elucidate the energy distribution of fast radio bursts. Additionally, Li et al. (2021) found that the bimodality of the energy

distribution of a fast radio burst is clearly time dependent. Thus, further long-term monitoring of giant and bright pulses is required to reveal their time-dependency.

In certain pulsars, there are coherent movements of subpulses across the pulse phase window, as defined by averages of a larger number of pulses (Weltevrede et al. 2006). The phenomenon of classical subpulse drifting is attributed to the circulation of sub-beams of emission around the magnetic axis. This occurs as a consequence of the $E \times B$ drift of spark plasma filaments, following the traditional vacuum gap model (Ruderman & Sutherland 1975). The bright pulse emission in the leading and trailing components of PSR B1133+16 presents a regular phase modulation. Also, one point that needs attention is that the leading and trailing strong pulses are not consecutive, but separated by normal pulses or nulls randomly. However, the classical drifting in subpulses is only detected for successive single pulses. To the best of our knowledge, there has been no similar regular phase drifting in bright pulses discovered. It is plausible to consider that the modulation should be examined within the context of electric fluctuations occurring throughout the entire magnetosphere. A joint study of the giant pulses from the Crab pulsar at radio and $\gamma$-ray suggests that the giant pulses originate from multiple concentrated emission regions (Lundgren et al. 1995). In the modified vacuum gap model, the thermal ions or electrons from the polar cap, along with the inflow of magnetospheric electron-positron pair plasma, contribute partially to the bright single pulse emission (Gil et al. 2003). The number of charges partaking in the coherence radiation is enhanced to give rise to high intensity emission. Simultaneously, the greater electric potential is responsible for the phase drifting in bright pulses.

## 5. Concluding Remarks

We have conducted a thorough analysis of high-quality individual-pulse data obtained from PSR B1133+16 at 322 MHz using GMRT. Throughout a continuous observation period of 7.45 hr, a total of 1082 bright pulses were detected. Our findings indicate several distinct characteristics of these bright pulses. The peak flux density ratio of strong pulses to the average pulse profile falls within the range of 10–23. The majority of strong pulses are concentrated around the longitudes corresponding to the leading and trailing windows of the mean pulse profile. Specifically, the ratio of the number of bright pulses in these regions is approximately 2.74. The distribution of pulse energy for each individual pulse can be characterized by a combination of two Gaussian components and a cutoff power-law with an index of $\alpha = -3.2$. No bright pulses with relative pulse energies exceeding 10 have been detected. Additionally, the bright pulses are slightly narrower compared to the mean pulse profile, and significantly broader than giant pulses. These observational results indicate that bright pulses and giant pulses have distinct physical origins,

and these observations provide valuable insights into the characteristics of bright pulses emitted by PSR B1133+16 at 322 MHz.

The regular phase modulation in bright pulses may be explained by the enhanced number of charges partaking in the coherent radiation process. The emission behaviors of bright pulses may provide a very important clue to understanding the underlying mechanism of bright pulse emission. Additional work of interest would include polarimetric observations at multifrequency to simultaneously explore the detailed statistical distributions of bright pulses. The Five-hundred-meter Aperture Spherical radio Telescope (FAST) possesses unprecedentedly high-sensitivity at 1250 MHz (Li et al. 2018), which will lead to a more detailed and comprehensive understanding of the pulsar emission mechanism. Combining the data from FAST and GMRT allows for multi-wavelength studies to establish the broadband nature of the phase drifting in bright pulses, and investigate the temporal evolution of drifting.

## Acknowledgments

## ORCID iDs

Zhi-Gang Wen ● https://orcid.org/0000-0003-2991-7421
Vishal Gajjar ● https://orcid.org/0000-0002-8604-106X
Wen-Ming Yan ● https://orcid.org/0000-0002-7662-3875

## References

Backer, D. C. 1973, ApJ, 182, 245
Bhat, N. D. R., Cordes, J. M., Camilo, F., Nice, D. J., & Lorimer, D. R. 2004, ApJ, 605, 759
Bhat, N. D. R., Tingay, S. J., & Knight, H. S. 2008, ApJ, 676, 1200
Bhattacharyya, B., Roy, J., Johnson, T. J., et al. 2021, ApJ, 910, 160
Bhattacharyya, B., Roy, J., Ray, P. S., et al. 2013, ApJL, 773, L12
Burke-Spolaor, S., Johnston, S., Bailes, M., et al. 2012, MNRAS, 423, 1351
Cheng, K. S., Ho, C., & Ruderman, M. 1986, ApJ, 300, 522
Cognard, I., Shrauner, J. A., Taylor, J. H., & Thorsett, S. E. 1996, ApJL, 457, L81
Cordes, J. M., Bhat, N. D. R., Hankins, T. H., McLaughlin, M. A., & Kern, J. 2004, ApJ, 612, 375
Cordes, J. M., & Lazio, T. J. W. 2002, arXiv:astro-ph/0207156
Enoto, T., Terasawa, T., Kisaka, S., et al. 2021, Sci, 372, 187
Ershov, A. A., & Kuzmin, A. D. 2005, A&A, 443, 593
Gil, J., Melikidze, G. I., & Geppert, U. 2003, A&A, 407, 315
Hankins, T. H., & Eilek, J. A. 2007, ApJ, 670, 693
Hankins, T. H., Kern, J. S., Weatherall, J. C., & Eilek, J. A. 2003, Natur, 422, 141
Herfindal, J. L., & Rankin, J. M. 2007, MNRAS, 380, 430
Honnappa, S., Lewandowski, W., Kijak, J., et al. 2012, MNRAS, 421, 1996
Istomin, Y. N. 2004 Young Neutron Stars and Their Environments Vol. 218 ed. F. Camilo & B. M. Gaensler, 369
Ji-Guang, L., Yuan-Jie, D., Long-Fei, H., et al. 2015, arXiv:1511.08298
Johnston, S., & Romani, R. W. 2002, MNRAS, 332, 109
Johnston, S., & Romani, R. W. 2003, ApJL, 590, L95
Johnston, S., & Romani, R. W. 2004 Young Neutron Stars and Their Environments Vol. 218 ed. F. Camilo & B. M. Gaensler, 315
Joshi, B. C., Kramer, M., Lyne, A. G., McLaughlin, M. A., & Stairs, I. H. 2004, in IAU Symposium, Vol. 218, Young Neutron Stars and Their Environments, ed. F. Camilo & B. M. Gaensler, Vol. 218 (San Francisco, CA: ASP), 319
Kargaltsev, O., Pavlov, G. G., & Garmire, G. P. 2006, ApJ, 636, 406
Karuppusamy, R., Stappers, B. W., & Lee, K. J. 2012, A&A, 538, A7
Karuppusamy, R., Stappers, B. W., & Serylak, M. 2011, A&A, 525, A55
Kazantsev, N. A., & Potapov, V. A. 2015, ATsir, 1628, 1
Knight, H. S., Bailes, M., Manchester, R. N., & Ord, S. M. 2005, ApJ, 625, 951
Kontorovich, V. M. 2009, arXiv:0911.3272
Kramer, M., Karastergiou, A., Gupta, Y., et al. 2003, A&A, 407, 655
Kuzmin, A. D., & Ershov, A. A. 2004, A&A, 427, 575
Kuzmin, A. D., & Ershov, A. A. 2006, AstL, 32, 583
Li, D., Wang, P., Qian, L., et al. 2018, IMMag, 19, 112
Li, D., Wang, P., Zhu, W. W., et al. 2021, Natur, 598, 267
Lorimer, D. R., & Kramer, M. 2012, Handbook of Pulsar Astronomy (Cambridge: Cambridge Univ. Press)
Lundgren, S. C., Cordes, J. M., Ulmer, M., et al. 1995, ApJ, 453, 433
Luo, R., Lee, K., Lorimer, D. R., & Zhang, B. 2018, MNRAS, 481, 2320
Luo, R., Men, Y., Lee, K., et al. 2020, MNRAS, 494, 665
Machabeli, G., Chkheidze, N., & Malov, I. 2019, Astrophysics and Space Science, 364, 40
Malov, I. F. 2022, ARep, 66, 12
Manchester, R. N., Hobbs, G. B., Teoh, A., & Hobbs, M. 2005, AJ, 129, 1993
Petrova, S. A. 2004, A&A, 424, 227
Ritchings, R. T. 1976, MNRAS, 176, 249
Romani, R. W., & Johnston, S. 2001, ApJL, 557, L93
Roy, J., Gupta, Y., Pen, U.-L., et al. 2010, ExA, 28, 25
Ruderman, M. A., & Sutherland, P. G. 1975, ApJ, 196, 51
Singal, A. K., & Vats, H. O. 2012, AJ, 144, 155
Staelin, D. H., & Reifenstein, E. C., III 1968, Sci, 162, 1481
Swarup, G., Ananthakrishnan, S., Kapahi, V. K., et al. 1991, CSci, 60, 95
Tao, G.-C., Esamdin, A., Hu, H.-D., et al. 2012, RAA, 12, 1649
Ulyanov, O. M., Zakharenko, V. V., Konovalenko, A. A., et al. 2006, IAU Joint Discussion, 2, 12
Vivekanand, M. 1995, MNRAS, 274, 785
Wang, F. Y., Zhang, G. Q., & Dai, Z. G. 2021, MNRAS, 501, 3155
Weltevrede, P., Edwards, R. T., & Stappers, B. W. 2006, A&A, 445, 243
Weltevrede, P., Stappers, B. W., & Edwards, R. T. 2007, A&A, 469, 607
Wen, Z. G., Yuan, J. P., Wang, N., et al. 2022, ApJ, 929, 71
Wen, Z. G., Yuen, R., Wang, N., et al. 2021, ApJ, 918, 57
Zhang, R. C., Zhang, B., Li, Y., & Lorimer, D. R. 2021, MNRAS, 501, 157